Louisiana State University

LSU Digital Commons

1-1-1997

Techniques for detecting gravitational waves with a spherical antenna

Stephen M. Merkowitz
Louisiana State University

Warren W. Johnson
Louisiana State University

Follow this and additional works at: https://digitalcommons.lsu.edu/physics_astronomy_pubs

Recommended Citation

The TIGA technique for detecting gravitational waves with a spherical antenna

Stephen M. Merkowitz* and Warren W. Johnson

Department of Physics and Astronomy, Louisiana State University, Baton Rouge, Louisiana 70803

(October 15, 2018)

We report the results of a theoretical and experimental study of a spherical gravitational wave antenna. We show that it is possible to understand the data from a spherical antenna with 6 radial resonant transducers attached to the surface in the truncated icosahedral arrangement. We find that the errors associated with small deviations from the ideal case are small compared to other sources of error, such as a finite signal-to-noise ratio. An *in situ* measurement technique is developed along with a general algorithm that describes a procedure for determining the direction of an external force acting on the antenna, including the force from a gravitational wave, using a combination of the transducer responses. The practicality of these techniques was verified on a room-temperature prototype antenna.

PACS numbers: 04.80.Nn, 06.70.Dn

I. INTRODUCTION

Techniques to directly detect gravitational waves have been under study for more than 25 years [1]. Two different methods are aggressively being pursued today: large laser interferometers, such as the proposed LIGO [2], and cryogenic resonant mass antennas, such as the operating ALLEGRO [3] and NAUTILUS [4] detectors. While most past work on resonant antennas has been with the original Weber bar type [5], large spherical antennas have recently been proposed and become of interest [6].

Several characteristics of a spherical antenna make it a unique and interesting instrument. First, it is omnidirectional, capable of detecting gravitational waves from all directions and polarizations. In addition, only a single spherical antenna is necessary for determining the direction of an incident gravitational wave. A sphere has a larger cross section than an equivalent bar [7]. A sphere can measure all the tensorial components of a gravitational wave, thus it is capable of testing different metric theories of gravity [8]. Finally, almost all of the more than 25 years of experience gained on bar antennas (cryogenics, resonant transducers, suspension,...) can be applied to a spherical antenna.

We begin this paper by reviewing the interaction between an elastic sphere and a gravitational wave. We start in Sec. II by describing how the gravitational field can be decomposed into 5 quadrupole components that will have a one-to-one correspondence with the quadrupole modes of a sphere as described in Sec. III.

When we first began this problem [9,10] we developed a model for a spherical antenna with 6 resonant mass motion sensors attached to the sphere surface at special locations. This model was limited because it put relatively strong constraints on the motion sensors. In order to further investigate the behavior of a more realistic antenna, it was necessary to generalize the model. In Sec. IV we develop a more general description of the detector by keeping the number, tuning, and arrangement of the motion sensors arbitrary. Section V shows how the response of the motion sensors can be used to observe the 5 quadrupole modes of the sphere and in Sec. VI we describe how this information can be used to determine the direction of an external excitation, including that from a gravitational wave.

In Sec. VII we show how the general equations of motion can be greatly simplified if a special arrangement of motion sensors is used. This system was the basis for our original model which we called a truncated icosahedral gravitational wave antenna (TIGA) [9]. The arrangement of resonators was similarly called the truncated icosahedral (TI) arrangement [10].

Other arrangements of transducers have been suggested [11,12], however, we feel the TI arrangement is advantageous not only because it simplifies the equations of motion but because it maintains equal sensitivity to gravitational waves from all directions and polarizations. We have also found that it facilitates in the interpretation of the signal from the motion sensors. In addition, it has been shown that in the presence of noise the use of 6 resonant transducers in the TI arrangement, compared to that of one for bar antenna, do not reduce the overall sensitivity of the antenna [9,13] and that the arrangement is fairly robust to the failure of a single motion sensor [14,15].

---

*Present affiliation ROG collaboration and the INFN Laboratori Nazionali di Frascati, Italy

In an actual antenna, it may be difficult to achieve a perfect TI arrangement. The motion sensors can be misplaced, mistuned, etc. To account for this we develop a measurement technique in Sec. VIII that takes into account any small deviations from the ideal arrangement. The results of a numerical simulation are also presented that show this technique to be accurate within reasonable levels of precision set for the detector components.

We begin discussion of experiments performed on a prototype spherical antenna in Sec. IX. The results of the prototype without resonators attached is reviewed in Sec. X. The behavior of the prototype with resonant transducers attached is presented in Sec. XI. To demonstrate the validity of the TIGA techniques in a single test, we show that from the response of the motion sensors, we can determine the location of an impulse excitation applied to the prototype's surface. This same procedure can be applied to determine the direction of a gravitational wave as discussed in Sec. VI.

II. QUADRUPOLE DECOMPOSITION OF THE GRAVITATIONAL FIELD

A gravitational wave is a traveling time-dependent deviation of the metric tensor, denoted by $h_{\mu\nu}$. We follow a common textbook development for the metric deviation of a gravitational wave, which finds that only the spatial components, h_{ij}, are non-zero, and further can be taken to be transverse and traceless [1]. The tensor is simplified if we initially write it in the "wave-frame", denoted by primed coordinates and indices. It is a coordinate frame with origin at the center of mass of the detector, and the z'-axis aligned with the propagation direction of the wave. Since we restrict ourselves to detectors much smaller than the gravitational wavelength, only the time dependence of $h_{i'j'}$ will have significant physical effects. Thus, the most general possible form for the spatial components of the metric deviation in the wave-frame can be written as:

$$
h_{i'j'}(t) = \begin{bmatrix} h'_+(t) & h'_\times(t) & 0 \\ h'_\times(t) & -h'_+(t) & 0 \\ 0 & 0 & 0 \end{bmatrix}
\tag{1}
$$

where $h'_+(t)$ and $h'_\times(t)$ are the time-dependent gravitational wave amplitudes for the two allowed states of linear polarization, and are called the plus and cross amplitudes.

The detector is more easily described in the "lab-frame", denoted by unprimed coordinates and indices, with origin also at the center of mass of the detector, and z-axis aligned with the local vertical. In this frame, the primary physical effect of a passing gravitational wave is to produce a time dependent "tidal" force density $f^{\mathrm{GW}}(\boldsymbol{x}, t)$ on material at coordinate location x_i with mass density ρ, which is related to the metric perturbation by

$$
f_i^{\mathrm{GW}}(\boldsymbol{x}, t) = \frac{1}{2}\rho \sum_j \frac{\partial^2 h_{ij}(t)}{\partial t^2} x_j.
\tag{2}
$$

We notice that this force can be written as the gradient of a time-dependent scalar potential:

$$
f_i^{\mathrm{GW}}(\boldsymbol{x}, t) = \nabla_i \Phi(\boldsymbol{x}, t) = \nabla_i \left(\sum_{j,k} \frac{1}{4}\rho x_j \ddot{h}_{jk}(t) x_k \right).
\tag{3}
$$

This scalar potential is a quadratic form in the spatial coordinates. It is natural to look for an alternate expression that separates the coordinate dependence into radial and angular parts. Because the tensor h_{ij} is traceless, the angular expansion can be done completely with the five ordinary spherical harmonics of order 2, which we denote by $Y_m(\theta, \phi)$ or Y_m. We call the resulting time dependent expansion coefficients, denoted by $h_m(t)$, the "spherical gravitational amplitudes." They are a complete and orthogonal representation of the cartesian metric deviation tensor $h_{ij}(t)$. They depend only on the two wave-frame amplitudes and the direction of propagation, and are defined by

$$
\Phi(\boldsymbol{x}, t) = \sqrt{\frac{\pi}{15}}\rho r^2 \sum_m \ddot{h}_m(t) Y_m.
\tag{4}
$$

The spherical harmonics Y_m can be any linear combination or rotation of the standard spherical harmonics of order 2, as long as the orthogonality between them is maintained. The advantage of not using the standard spherical harmonics will become apparent later, but for an example of an alternative set and their relation to a lab frame see reference [10].

The 5 orthogonal spherical amplitudes h_m are a complete set of measurable quantities of the local gravitational field. Once a proper relation to the lab coordinate system is defined, the determination of the source direction follows immediately by inversion of this relationship [16].

2

By examining Eq. (3) closely, we note that because the force is a quadratic it is the equation of an ellipsoid. Therefore, we can picture a gravitational wave as a time-dependent ellipsoidal deformation of the local coordinates. While this may seem obvious, we note it here as this is a very useful visual tool for understanding the interaction between a gravitational wave and the detector. We discuss this idea in more detail below to show the connection with other quadratic quantities.

III. THE UNCOUPLED SPHERE

The mechanics of a general antenna can be described by ordinary elastic theory. Forces acting on the body will cause a deformation described by the displacement vector $\boldsymbol{u}(\boldsymbol{x}, t)$, where $\boldsymbol{x}$ is the equilibrium position of a mass element. The equations of motion are then

$$\rho \frac{\partial^2 \boldsymbol{u}}{\partial t^2} = (\lambda + \mu) \boldsymbol{\nabla}(\boldsymbol{\nabla} \cdot \boldsymbol{u}) + \mu \boldsymbol{\nabla}^2 \boldsymbol{u} + \sum \boldsymbol{f}, \tag{5}$$

where the Lamé coefficients λ and μ specify the elastic stiffness of the material and $\sum \boldsymbol{f}$ represents the sum of external force densities acting on the body [17].

In this paper, we include two forces in $\sum \boldsymbol{f}$. First, the signal or gravitational force density $\boldsymbol{f}^{\mathrm{GW}}$ from Eq. (2). Second, if objects are attached to the antenna, there will exist a reaction force between the object and the surface of the antenna. Thus we choose to express the coupling to other objects, such as secondary resonators, as if they were external forces in Eq. (5). This device lets us partition the equations of motion in a convenient way.

A solution to the differential Eq. (5) can be found by the standard eigenfunction expansion. This allows a separation of the spatial and time dependence of the displacement vector

$$\boldsymbol{u}(\boldsymbol{x}_i, t) = \sum_m a_m(t) \boldsymbol{\Psi}_m(\boldsymbol{x}_i). \tag{6}$$

Each spatial eigenfunction, $\boldsymbol{\Psi}_m(\boldsymbol{x})$, is the time independent part of the solution for unforced harmonic oscillation at the eigenfrequency ω_m, and is found by solving

$$-\rho \omega_m^2 \boldsymbol{\Psi}_m = (\lambda + \mu) \boldsymbol{\nabla}(\boldsymbol{\nabla} \cdot \boldsymbol{\Psi}_m) + \mu \nabla^2 \boldsymbol{\Psi}_m, \tag{7}$$

subject to the time-stationary boundary conditions, which for a sphere require that the total force per unit area at the surface vanish in the direction normal to the surface. The quantity $a_m(t)$ is the time-dependent mode amplitude. The mode index, m, enumerates the discrete set of modes, which obey the usual orthogonality property

$$\int_V \boldsymbol{\Psi}_m(\boldsymbol{x}) \cdot \boldsymbol{\Psi}_n(\boldsymbol{x}) d^3 x = N_m \delta_{mn}. \tag{8}$$

The normalization constant N_m is arbitrary, however, in the case of a sphere of radius R we define it to be

$$N_m \equiv \frac{4}{3} \pi R^3. \tag{9}$$

Combining the equations above, and using orthogonality to eliminate the summation, we find the standard result, one forced harmonic oscillator equation for each mode amplitude,

$$\ddot{a}_m(t) + \omega_m^2 a_m(t) = \frac{1}{\rho N_m} \int \boldsymbol{\Psi}_m(\boldsymbol{x}) \cdot \sum \boldsymbol{f}(\boldsymbol{x}, t) d^3 x. \tag{10}$$

The mode amplitudes are a complete set of collective coordinates for the description of the antenna motion. All the interactions with the outside world, including gravitation, can be included as separate terms in the "effective force" on each mode. An efficient approximation scheme will use only those modes needed for an accurate description of the antenna. Only a few of the "overlap integrals" with $\boldsymbol{f}^{\mathrm{GW}}$ in Eq. (10) are large, therefore, only a few of the mode amplitudes are strongly coupled to gravitational waves.

Let us consider the case a perfectly homogeneous and isotropic sphere uncoupled from the outside world. This should give a reasonable approximation to the behavior of a sphere where all the external forces are small. The eigenfunctions for this case were found over a hundred years ago [18,19], however, more elegant derivations, using modern notation are available [7,20].

3

The eigenfunctions of a sphere can be described in terms of spherical harmonics $Y_{\ell m}(\theta, \phi)$. Looking at the overlap integral in Eq. (10), we see that we need only consider odd-parity modes. For a sphere of radius R the eigenfunctions are written:

$$\boldsymbol{\Psi}_{\ell m} = [\alpha_\ell(r)\hat{\boldsymbol{r}} + \beta_\ell(r)R\boldsymbol{\nabla}]\, Y_{\ell m}(\theta, \phi), \ \ell \text{ even.} \tag{11}$$

The radial eigenfunctions $\alpha_\ell(r)$ and $\beta_\ell(r)$ determine the motion in the radial and tangential directions respectively. There are 5 quadrupole modes of vibration which strongly couple to the force density of a gravitational wave, and are all degenerate, having the same angular eigenfrequency ω_o. They are distinguished only by their angular dependence. For the remainder of this discussion we only consider the quadrupole ($\ell = 2$) modes so we drop the ℓ in our notation.

The radial eigenfunctions are given by Ashby and Dreitlein [20]:

$$\alpha(r) = cR\frac{\partial}{\partial r}j_2(qr) + 6dR\frac{1}{r}j_2(kr) \tag{12}$$

$$\beta(r) = cj_2(qr) + d\frac{\partial}{\partial r}\left[rj_2(kr)\right], \tag{13}$$

where j_2 is the spherical Bessel function of order 2. The longitudinal and transverse wave vectors are given by $q^2 = \rho\omega_o^2/(\lambda + 2\mu)$ and $k^2 = \rho\omega_o^2/\mu$ respectively. The boundary conditions

$$c\frac{d}{dr}\left[\frac{j_2(qr)}{r}\right] + d\left[\frac{5}{r^2} - \frac{k^2}{2} - \frac{1}{r}\frac{d}{dr}\right]j_2(kr)\Bigg|_{r=R} = 0, \tag{14}$$

$$c\left[\frac{6}{r^2} - \frac{k^2}{2} - \frac{2}{r}\frac{d}{dr}\right]j_2(qr) + 6d\frac{d}{dr}\left[\frac{j_2(kr)}{r}\right]\Bigg|_{r=R} = 0, \tag{15}$$

determine the uncoupled mode frequency ω_o. Inclusion of the normalization condition Eq. (9) determines the constants c and d. These coefficients specify the shape of the eigenfunctions and are all weakly dependent on Poisson's ratio [7,10].

The gravitational effective force for mode m of the sphere, F_m^S, from Eq. (10) is

$$F_m^S \equiv \int_{V_o} \boldsymbol{\Psi}_m \cdot \boldsymbol{f}^{\mathrm{GW}}\, d^3x. \tag{16}$$

Solving the integrals, using Eqs. (3) and (11), we find

$$\begin{aligned} F_m^S(t) &= \sqrt{\frac{4\pi}{15}}\rho\ddot{h}_m(t)R^4\left[cj_2(qR) + 3dj_2(kR)\right] \\ &= \frac{1}{2}\ddot{h}_m(t)\,m_S\,\chi R. \end{aligned} \tag{17}$$

Thus we find that each spherical component of the gravitational field determines uniquely the effective force on the corresponding mode of a sphere, and they are all identical in magnitude. We can interpret the effective force F_m^S in each mode as the product of: the physical mass of the sphere m_S, an effective length χR, and the gravitational acceleration $\frac{1}{2}\ddot{h}_m$. The factor χ is a weak function of Poisson's Ratio [10].

We now see why it was convenient to write the gravitational wave amplitudes in terms of spherical harmonics: we have a clear way to make the connection between the gravitational strain h_m, the force they apply to the sphere modes F_m, and the amplitudes of the sphere's quadrupole modes a_m. There is a one-to-one correspondence between these three quantities when the same set of spherical harmonics are used. Once we know any of these quantities, we can immediately infer the other two. Later in this paper we will add one more quantity to this list, "mode channels" which are constructed from the observables of the antenna to have a one-to-one correspondence with the above quantities.

As in the case of the quadratic form of the gravitational field discussed above, the spherical harmonics Y_m can be any linear combination or rotation of the standard spherical harmonics of order 2, as long as orthogonality between them is maintained. The advantage here is that if the 5 quadrupole modes are not degenerate, but have "fixed" themselves in a particular orientation, one can choose an appropriate set of spherical harmonics that match the actual orientation of the quadrupole modes relative to the lab frame. This basis set can then be used to describe the gravitational field to maintain the one-to-one connection between the spherical amplitudes and the 5 quadrupole modes of the sphere.

Also analogous to the spherical amplitudes, the deformation of the sphere due to the excitation of a quadrupole normal mode can be described by the quadratic equation of an ellipsoidal surface. We recall that the geometry of

an ellipsoid can be visualized by the principal axis theorem. It shows that the general ellipsoid has three orthogonal axes that pierce the surface at three principal radii, two of which are extremal points on the surface. The orientation of the axes are described by 3 parameters, such as Euler angles. The shape is described by the relative size of the principal radii. If we call dr_1, dr_2, and dr_3 the deviation of these radii from their average, then a true sphere has $dr_1 = dr_2 = dr_3 = 0$, an oblate (or prolate) ellipsoid has $dr_2 = dr_3 = -2dr_1$, and a triaxial ellipsoid has $dr_1 > dr_2 > dr_3$. Thus 6 parameters completely describe the geometry. However, there is one restriction on the ellipsoids describing the quadrupole modes: they are isovolumetric with the sphere, which requires $dr_1 + dr_2 + dr_3 = 0$, so that 5 parameters suffice. Since the superposition of any ellipsoid is another ellipsoid, the eigenfunctions $Y_1 \ldots Y_5$ form a complete and orthogonal basis set for a 5 dimensional abstract vector space that describes all possible isovolumetric ellipsoids and all possible quadrupolar vibrations of the sphere.

IV. SPHERE COUPLED TO AN ARBITRARY NUMBER OF RESONATORS

We have just shown that measurement of the quadrupole modes of a sphere measures all of the tensorial components of the gravitational field, but a simple spherical resonator is not a practical detector. One requirement for practicality is a set of secondary modes or mechanical resonators. All current bar antennas use resonators that interact only with the vector component of antenna motion normal to the surface on which they are mounted, thus it seems natural to restrict our consideration to resonators of this type.

We choose here to describe the sphere's quadrupole modes in the coupled system using the eigenfunctions derived above for the uncoupled sphere. Lobo and Serrano showed this approximation to be valid when the ratio of the mass of the sphere to the mass of a resonator is much less than one [11]. This approximation allows us to use a much more simple mathematical framework, without loss of generality, as all the proposed detectors [6] satisfy this requirement.

We look now at J number of resonators attached to the sphere surface at arbitrary angular positions (θ_j, ϕ_j). The values of the relative radial displacements of the sphere surface at the resonator locations can be grouped together into a "pattern vector" for a particular mode. These column vectors in turn may be collected together to form a "pattern matrix" B_{mj} defined by

$$B_{mj} \equiv \frac{1}{\alpha} \hat{\boldsymbol{r}} \cdot \boldsymbol{\Psi}_m (\theta_j, \phi_j), \tag{18}$$

where α is the radial eigenfunction given by Eq. (12) evaluated at the surface of the sphere. From Eq. (11) we find

$$B_{mj} = Y_m (\theta_j, \phi_j). \tag{19}$$

Because the eigenfunctions are invariant to reflection through the origin, we may restrict the location of resonators to one hemisphere, without loss of generality.

By mechanical resonator we mean a small elastic system that has one of its own normal modes tuned to be resonant with the frequency of the antenna. The antenna surface motion excites this mode, and there is resonant transfer of momentum between the resonator and the antenna. Hence it acts as a resonant mechanical transformer, turning small motions of the large antenna into large motions of the small resonator. Each resonator j is constructed to obey a one-dimensional harmonic oscillator equation:

$$m_j^r \ddot{q}_j(t) + m_j^r \sum_m \alpha B_{mj} \ddot{a}_m(t) + k_j^r q_j(t) = F_j^r(t). \tag{20}$$

The displacement of a resonator, relative to the sphere surface, is denoted by q_j. Any random or noise forces that act between the small resonator and the sphere are included in F_j^r. Under ideal circumstances we would assume that the resonators are identical, such that the mass m_j^r and spring constant k_j^r of each are tuned to match the frequency of the degenerate 5 sphere modes, however, at this point we wish to keep the equations general so we *do not* put any restrictions on these parameters.

Combining the above, we find the coupled equations of motion for the sphere modes are

$$m_m^s \ddot{a}_m(t) + k_m^s a_m(t) - \sum_j \alpha B_{mj} k_j^r q_j(t) = -\sum_j \alpha B_{mj} F_j^r(t) + F_m^s(t). \tag{21}$$

Again, under ideal circumstances we would assume that the 5 quadrupole modes of the sphere are degenerate so that the mass m_m^s and spring constant k_m^s of each mode are identical, however, at this point we wish to keep the equations general so we *do not* put any restrictions on these parameters.

It is convenient to combine Eqs. (20) and (21) into a matrix notation. We denote matrices by a double underscore and column vectors by a single underscore. We begin by defining the following diagonal matrices:

$$M^s_{jm} \equiv \delta_{jm}m^s_m, \quad M^r_{jm} \equiv \delta_{jm}m^r_j,$$
$$K^s_{jm} \equiv \delta_{jm}k^s_m, \quad K^r_{jm} \equiv \delta_{jm}k^r_j.$$

The complete set of coupled equations of motion can now be written:

$$\begin{bmatrix} \underline{\underline{M}}^s & \underline{\underline{0}} \\ \alpha\underline{\underline{M}}^r\underline{\underline{B}}^T & \underline{\underline{M}}^r \end{bmatrix}\begin{bmatrix} \underline{\ddot{a}}(t) \\ \underline{\ddot{q}}(t) \end{bmatrix} + \begin{bmatrix} \underline{\underline{K}}^s & -\alpha\underline{\underline{B}}\,\underline{\underline{K}}^r \\ \underline{\underline{0}} & \underline{\underline{K}}^r \end{bmatrix}\begin{bmatrix} \underline{a}(t) \\ \underline{q}(t) \end{bmatrix} = \begin{bmatrix} \underline{\underline{I}} & -\alpha\underline{\underline{B}} \\ \underline{\underline{0}} & \underline{\underline{I}} \end{bmatrix}\begin{bmatrix} \underline{F}^s(t) \\ \underline{F}^r(t) \end{bmatrix}. \tag{22}$$

The column vector $\underline{a}$ has 5 components, one for each sphere mode, and the column vector $\underline{q}$ has J components, one for each resonator. The dimensions of the constant matrices can be inferred from these two column vectors. The matrix $\underline{\underline{0}}$ is defined to have all elements equal to zero, and $\underline{\underline{I}}$ is the identity matrix.

These equations should give a good account of the mechanics of the system for arbitrary numbers and locations of resonators. We do not include terms which represent the "dissipation" part of friction, which can be shown to be negligible for the calculations we do here, however, we do include the "fluctuation" part of friction, within the random driving forces in $\underline{F}^s$ and $\underline{F}^r$.

We also do not include any deviations to the shape of the quadrupole modes. One possible cause for changes in shape is the the attachment of the resonators. This would obviously become a problem if very large resonators were used. However, as shown by Lobo and Serrano [11], if we limit ourselves to resonators with mass less than 1% of the sphere mass this effect becomes negligible. A second possible cause for a change in mode shape is a hole drilled through the sphere for suspension. However, finite element analysis of a sphere with a hole [21] as well as experiments [22,23] have shown the mode shapes to be changed by less than 1% due to the suspension hole.

It is clear that Eq. (22) represents a set of elastically coupled harmonic oscillators with driving forces. The apparent peculiarities (off-diagonal terms in the mass matrix and asymmetry in the elastic matrix) are simply artifacts of use of the non-inertial coordinates $\underline{q}$. However, we can greatly simplify these equations by transforming to a normal coordinate system. We begin by noting that Eq. (22) is of the form

$$\underline{\underline{M}}\,\underline{\underline{\gamma}}\,\underline{\ddot{y}}(t) + \underline{\underline{K}}\,\underline{\underline{\gamma}}\,\underline{y}(t) = \underline{\underline{R}}\,\underline{F}(t), \tag{23}$$

where we have defined

$$\underline{\underline{M}} \equiv \begin{bmatrix} \underline{\underline{M}}^s & \underline{\underline{0}} \\ \alpha\underline{\underline{M}}^r\underline{\underline{B}}^T & \underline{\underline{M}}^r \end{bmatrix}, \tag{24}$$

$$\underline{\underline{K}} \equiv \begin{bmatrix} \underline{\underline{K}}^s & -\alpha\underline{\underline{B}}\,\underline{\underline{K}}^r \\ \underline{\underline{0}} & \underline{\underline{K}}^r \end{bmatrix}, \tag{25}$$

$$\underline{\underline{R}} \equiv \begin{bmatrix} \underline{\underline{I}} & -\alpha\underline{\underline{B}} \\ \underline{\underline{0}} & \underline{\underline{I}} \end{bmatrix}, \tag{26}$$

and for convenience we have transformed to mass weighted coordinates $\underline{y}$ with the matrix $\underline{\underline{\gamma}}$. We can rewrite Eq. (23) as:

$$\underline{\ddot{y}}(t) + \underline{\underline{X}}\,\underline{y}(t) = \underline{\underline{\gamma}}^{-1}\underline{\underline{M}}^{-1}\underline{\underline{R}}\,\underline{F}(t), \tag{27}$$

where we have defined

$$\underline{\underline{X}} \equiv \underline{\underline{\gamma}}^{-1}\underline{\underline{M}}^{-1}\underline{\underline{K}}\,\underline{\underline{\gamma}}. \tag{28}$$

We may diagonalize $\underline{\underline{X}}$ using the transformation $\underline{\underline{D}} = \underline{\underline{U}}^{-1}\underline{\underline{X}}\,\underline{\underline{U}}$. We now define our normal coordinates as $\underline{\eta}(t) \equiv \underline{\underline{U}}^{-1}\underline{y}(t)$. For convenience, we also define a transformation matrix $\underline{\underline{V}} \equiv \underline{\underline{\gamma}}\,\underline{\underline{U}}$. Substituting these into Eq. (27) and multiplying the entire expression by $\underline{\underline{U}}^{-1}$ we find

$$\underline{\ddot{\eta}}(t) + \underline{\underline{D}}\,\underline{\eta}(t) = \underline{\underline{V}}^{-1}\underline{\underline{M}}^{-1}\underline{\underline{R}}\,\underline{F}(t). \tag{29}$$

The problem has now been reduced to $5 + J$ decoupled harmonic oscillator equations. To solve them we begin by taking the Fourier transform of Eq. (29)

6

$$\underline{\underline{G}}^{-1}(\omega)\underline{\eta}(\omega) = \underline{\underline{V}}^{-1}\underline{\underline{M}}^{-1}\underline{\underline{R}}\,\underline{F}(\omega), \tag{30}$$

where we have defined

$$\underline{\underline{G}}^{-1}(\omega) \equiv \underline{\underline{D}} - \omega^2 \underline{\underline{I}}. \tag{31}$$

Because $\underline{\underline{D}}$ is diagonal, $\underline{\underline{G}}^{-1}(\omega)$ is also diagonal, so its inverse is just the diagonal elements inverted. We can now easily solve for the normal coordinates:

$$\underline{\eta}(\omega) = \underline{\underline{G}}(\omega)\underline{\underline{V}}^{-1}\underline{\underline{M}}^{-1}\underline{\underline{R}}\,\underline{F}(\omega). \tag{32}$$

To return to the original coordinates we reverse the transformations:

$$\begin{bmatrix} \underline{a}(\omega) \\ \underline{q}(\omega) \end{bmatrix} = \underline{\underline{\gamma}}\,\underline{y}(\omega) \tag{33}$$

$$= \underline{\underline{V}}\,\underline{\eta}(\omega) \tag{34}$$

$$= \underline{\underline{V}}\,\underline{\underline{G}}(\omega)\,\underline{\underline{V}}^{-1}\underline{\underline{M}}^{-1}\underline{\underline{R}}\,\underline{F}(\omega). \tag{35}$$

Note that Eq. (34) provides a convenient way to transform to normal modes where the frequency response is simple. The matrix $\underline{\underline{V}}$ is always invertible as we know the inverse of $\underline{\underline{U}}$ and $\underline{\underline{\gamma}}$ exist, thus making it possible to transform in both directions. This transformation will be important in the final analysis of the detector discussed below.

V. MODE CHANNELS

In our original TIGA model [9] we showed it was possible to combine the observable resonator displacements $\underline{q}(t)$ into a quantity which we called "mode channels" because they have a one-to-one correspondence with the quadrupole modes of a sphere, and thus the spherical amplitudes of a gravitational wave. It is desirable at this point to develop a general expression for the equivalent of mode channels for any number and arrangement of radial resonant transducers.

We begin by taking the Fourier transform of Eqs. (20) and (21):

$$\left[\underline{\underline{K}}^r - \omega^2\underline{\underline{M}}^r\right]\underline{q}(\omega) - \alpha\omega^2\underline{\underline{M}}^r\underline{\underline{B}}^T\underline{a}(\omega) = \underline{F}^r(\omega) \tag{36}$$

$$\left[\underline{\underline{K}}^s - \omega^2\underline{\underline{M}}^s\right]\underline{a}(\omega) - \alpha\underline{\underline{B}}\,\underline{\underline{K}}^r\underline{q}(\omega) = -\alpha\underline{\underline{B}}\,\underline{F}^r(\omega) + \underline{F}^s(\omega) \tag{37}$$

For the moment, we are only interested in the force of the gravitational wave acting on the sphere, so we will assume to have a high signal-to-noise ratio, thus we can ignore the external forces on the resonators and set $\underline{F}^r(\omega) = 0$. We can now solve for $\underline{F}^s(\omega)$ in terms of $\underline{q}(\omega)$

$$\underline{F}^s(\omega) = \left[\frac{1}{\alpha\omega^2}\underline{\underline{K}}^s\left(\underline{\underline{B}}\,\underline{\underline{M}}^r\underline{\underline{B}}^T\right)^{-1}\underline{\underline{B}}\,\underline{\underline{K}}^r - \frac{1}{\alpha}\underline{\underline{K}}^s\left(\underline{\underline{B}}\,\underline{\underline{M}}^r\underline{\underline{B}}^T\right)^{-1}\underline{\underline{B}}\,\underline{\underline{M}}^r \right.$$
$$\left. - \frac{1}{\alpha}\underline{\underline{M}}^s\left(\underline{\underline{B}}\,\underline{\underline{M}}^r\underline{\underline{B}}^T\right)^{-1}\underline{\underline{B}}\,\underline{\underline{K}}^r + \frac{\omega^2}{\alpha}\underline{\underline{M}}^s\left(\underline{\underline{B}}\,\underline{\underline{M}}^r\underline{\underline{B}}^T\right)^{-1}\underline{\underline{B}}\,\underline{\underline{M}}^r - \alpha\underline{\underline{B}}\,\underline{\underline{K}}^r\right]\underline{q}(\omega) \tag{38}$$

Eq. (38) gives us the means, using the observable resonator displacements $\underline{q}$, to infer the force on the quadrupole modes applied by a gravitational wave. However, the complicated frequency response will make its implementation difficult because all the parameters on the right hand side must be known. While it may be possible to determine all of these parameters (see the Appendix for an example) we would prefer a technique that is not so strongly dependent upon measuring these. In addition, we would prefer an arrangement where the frequency response can be simplified.

In the following sections we propose an alternative technique that does not require one to know all the parameters of the detector to high accuracy. Using a special symmetric arrangement of resonators, the above equations can be simplified. Along with a special procedure, possibly unique to this arrangement, we can obtain all the information about the external forces without knowing all the parameters of the system to high accuracy.

VI. DIRECTION FINDING TECHNIQUE

A. General technique

It is very desirable to demonstrate a general algorithm for finding the location of an arbitrary excitation solely from the mode channel amplitudes. We were able to find and successfully test such an algorithm, one suggested by the ellipsoidal picture for the shape of the modes discussed above.

The measured amplitudes of the quadrupole modes directly tell us the relative amounts of each of the 5 basis ellipsoids that must be superimposed to get the net ellipsoidal deformation. We denote the 5 ellipsoidal amplitudes by h_m, and call them the vibration amplitudes in the "spherical representation."

We can also define a matrix of the quadratic form h_{ij} whose elements form a complete set of amplitudes in what we call the "cartesian representation." The connection between representations is easily found to be

$$h_{ij}(t) = \begin{bmatrix} h_{xx} & h_{xy} & h_{xz} \\ h_{yx} & h_{yy} & h_{yz} \\ h_{zx} & h_{zy} & h_{zz} \end{bmatrix}$$
$$= \begin{bmatrix} h_1 - \frac{1}{\sqrt{3}}h_5 & h_2 & h_4 \\ h_2 & -h_1 - \frac{1}{\sqrt{3}}h_5 & h_3 \\ h_4 & h_3 & \frac{2}{\sqrt{3}}h_5 \end{bmatrix}. \tag{39}$$

The connection between this representation and the geometry of ellipsoids comes again from the principal axes theorem, which states that the three eigenvectors of the matrix h_{ij} are parallel to the three principal axes, and the radial deviations dr_i are the corresponding eigenvalues of h_{ij}.

An excitation can be classified by the shape and orientation of the ellipsoid it produces. Once this shape is realized, one need only solve for the eigenvalues and eigenvectors of the matrix h_{ij} to determine the direction of the excitation. The exact interpretation of the eigenvalues and eigenvectors will of course depend upon the expected ellipsoidal deformation.

B. Inferring a gravitational wave's direction

The method described in the previous section can be used to determine the direction of an incident gravitational wave. As shown in Sec. II, the gravitational field can also be represented by an ellipsoid derived from the electric components of the Riemann tensor [24,25]. It describes the relative acceleration of gravity that causes an ellipsoidal deformation of an initially spherical group of free test particles. In a conventional gauge, that ellipsoid is also described by the 9 spatial components of the gravitational strain tensor h_{ij} in cartesian coordinates. It can easily be shown that this tensor is in exact one-to-one correspondence to the cartesian amplitudes of vibration of the sphere, so in this paper we have used the same symbol h_{ij} for both.

Now, the direction problem in gravitation requires only knowledge of what sort of ellipsoid is produced by a gravitational wave. By examining the conventional description of the strain tensor of a wave according to General Relativity [26], we find that one principal axis of the ellipsoid is aligned with the direction of propagation, and that the corresponding radial deviation is zero. Therefore, we need only determine the wave's ellipsoid, and then we know the eigenvector of the zero eigenvalue points at the source. (This position determination is unique only within a hemisphere; sources in diametrically opposite directions are indistinguishable.)

Note that this method does not require intensive calculations, such as those used to compute the maximum likelihood estimates performed by Zhou and Michelson [12]; however, its effectiveness in the presence of noise still needs to be evaluated.

C. Inferring the direction of a radial impulse

Since a laboratory source of gravitational waves does not exist, we need an alternative type of excitation for testing this technique. We find that a radial impulse to the surface of a sphere is a good substitute.

We present here a simple picture of the antenna's response to a radial impulse. Suppose a sphere has a degenerate quadrupole mode multiplet, so we are free to choose a basis set with *arbitrary* orientation to describe it. If we choose an orientation with the z'-axis of the mode frame to be along the direction of the impulse, then only a *single* mode (Y_5)

in that frame will be excited (all of the other modes have a vanishing radial component of their eigenfunctions at this location, which makes their "overlap" integral with the impulse vanish). The corresponding ellipsoid produced is an oblate spheroid which has maximum radial deviation at the location of the impulse, and two half-size radial deviations of opposite sign in the orthogonal directions. Therefore, the location of the impulse is given by the eigenvector with the largest eigenvalue. This also provides a check for the assumed shape (in a measurement with a high signal-to-noise ratio) as the other two eigenvalues should be equal to each other, but half the size and opposite in sign of the first.

VII. THE IDEAL TRUNCATED ICOSAHEDRAL ARRANGEMENT

A. Symmetry

When we began this problem [9] we introduced a special arrangement of 6 resonators which we termed a Truncated Icosahedral Gravitational Wave Antenna (TIGA) shown in Fig. 1. We proposed using a truncated icosahedron as an approximation to a sphere, however the only requirement for the Truncated Icosahedral (TI) arrangement was that the resonant transducers be placed at positions on the surface of a sphere at the center of six non-antipodal pentagon faces of an imaginary truncated icosahedron (or dodecahedron) concentric to the sphere.

The original TIGA model [10] assumed perfect symmetry of the sphere as well as the tuning and placement of the resonant transducers. While the effects of deviations from perfect symmetry on a sphere's uncoupled quadrupole modes have been studied [11,22,23], we still need to investigate the effect of asymmetries on our ability to properly interpret the signals from resonant motion sensors. This is why we have kept the equations general until now. It is possible to investigate alternative arrangements of radial resonators, such as the one proposed by Lobo and Serrano [11], with the above framework, however, we will limit ourselves here to the TI arrangement for reasons stated in the introduction.

The symmetry of a TI, shown in Fig. 2, greatly simplifies various aspects of the problem; not only in the calculations that follow, but also in the construction of such a device. A TI has 32 flat surfaces suitable for mounting transducers, calibrators, balancing weights and suspension attachments. In addition, the symmetry makes machining the solid TI relatively simple [21]. However, as stated above, the only requirement is on the placement of the resonators, not on the shape of the "spherical" mass.

The high symmetry of the TI arrangement becomes apparent when you examine its pattern matrix $\underline{\underline{B}}$. Each pattern vector is orthogonal to the others, and each has the same magnitude, $\sqrt{\frac{3}{2\pi}}$, or in other words:

$$\underline{\underline{B}}\,\underline{\underline{B}}^T = \frac{3}{2\pi}\underline{\underline{I}}. \tag{40}$$

This property causes the cross terms between sphere modes in the normal mode eigenfunctions to vanish. In addition to the orthogonality, the sum of the components of each pattern vector vanishes:

$$\underline{\underline{B}}\,\underline{1} = \underline{0}. \tag{41}$$

The 6×1 column vector $\underline{1}$ is defined to have all elements equal to unity, while the 5×1 column vector $\underline{0}$ has all elements equal to zero.

B. Eigenfunction solution

The symmetry of the pattern matrix also suggested that there might be an analytic solution for the collection of eigenvectors $\underline{\underline{U}}$ and the eigenvalue matrix $\underline{\underline{D}}$ of Eq. (29). Examination of the numerical results suggested a likely form for $\underline{\underline{U}}$, and substitution in the equations verified that it was a solution and determined the values of the constants. The details of this solution can be found elsewhere [10,21].

It is convenient to divide the resulting set of eigenvectors, $\underline{\underline{U}}$, into three groups. The first two groups each contain 5 column eigenvectors and we denote them by $\underline{\underline{U}}_+$ and $\underline{\underline{U}}_-$:

$$\underline{\underline{U}}_\pm = n_\pm \left[\begin{array}{c} \underline{\underline{I}} \\ c_\pm \underline{\underline{B}}^T \end{array} \right]. \tag{42}$$

The physical interpretation of these is simple: each coupled eigenmode "mimics" the motion of one of the uncoupled sphere eigenmodes. In other words, each coupled resonator's radial motion is proportional to the uncoupled sphere

eigenfunctions at that resonator's location. This amplified version of a mode's pattern vector is either in-phase and down-shifted in frequency, or anti-phase and up-shifted in frequency. The frequency shifts are all identical, so that the quintuplet of degenerate bare sphere-modes has bifurcated into up-shifted and down-shifted degenerate quintuplets of modes. The amount of frequency shifting is given by the eigenvalues of $\underline{U}$, which are the diagonal elements of the matrix $\underline{\underline{D}}$. The identity matrix in Eq. (42) is an indication that energy will *not* be transferred from one sphere mode to another. The $\pm$ notation has been used on the dimensionless constants $n_\pm$ and $c_\pm$ as well to refer to the up $(+)$ or down $(-)$ shifting of the frequencies.

The remaining single eigenvector is

$$\underline{U}_o = \left[\begin{array}{c} \underline{0} \\ n_o \underline{1} \end{array} \right]. \tag{43}$$

This mode is at the original sphere frequency and does not strongly interact with a gravitational wave. All the resonators move in unison and the sphere modes do not move at all.

C. Ideal mode channels

Now let us see what the mode channels look like for the ideal TI arrangement:

$$\underline{\underline{M}}^s = m_s \underline{\underline{I}}, \ \underline{\underline{M}}^r = m_r \underline{\underline{I}},$$
$$\underline{\underline{K}}^s = k_s \underline{\underline{I}}, \ \underline{\underline{K}}^r = k_r \underline{\underline{I}},$$

thus

$$\underline{F}^s(\omega) = \left[\frac{2\pi}{3\alpha\omega^2 m_r} \left(k_s - \omega^2 m_s \right) \left(k_r - \omega^2 m_r \right) - \alpha k_r \right] \underline{\underline{B}} \, \underline{q}(\omega). \tag{44}$$

What is striking about Eq. (44) is that all the complicated frequency dependence has been separated from the matrices and a simple linear combination of the resonator responses can be made to obtain all the information about the external forces. We, therefore, define a quantity $\underline{g}$ which does not contain the complicated frequency dependence, but still maintains the one-to-one correspondence with the quadrupole components of the external force acting on the sphere:

$$\underline{g} \equiv \underline{\underline{B}} \, \underline{q}. \tag{45}$$

The components of the mode channels g_m can be used as a substitute for the amplitudes h_m in order to solve for the directional information of an excitation, such as a gravitational wave. A practical application of this technique for an impulse excitation to the surface of a prototype antenna will be described later in Sec. X.

D. Resonator ellipsoids

From the equations of motion of an ideal TIGA, we found that the eigenfunctions of the coupled modes were such that the motion of the resonators mimicked the ellipsoidal deformation of the sphere's surface either in phase or anti-phase. We, therefore, can picture the collective motion of the six resonators to describe six "resonator ellipsoids", 5 of which are mimicking the "quadrupole ellipsoids" of the sphere. The sixth resonator ellipsoid is just a sphere, where the six resonators are moving in unison with equal amplitude and phase, and the sphere surface does not move at all, as described by Eq. (43).

Each individual resonator now represents a superposition of the point radial deformation of the 6 resonator ellipsoids at a particular position. The transformation between point radial deformations $\underline{q}$ and ellipsoidal amplitudes $\underline{g}$ is given by the pattern matrix $\underline{\underline{B}}$ defined by the positions of the resonators and the orientation of the 5 quadrupole ellipsoids relative to a fixed lab frame:

$$\underline{g} = \underline{\underline{B}} \, \underline{q}. \tag{46}$$

Note that Eq. (46) is identical to Eq. (45) for transforming to mode channels. Through this discovery we realize that in the case of the TI arrangement, we can think of mode channels as the result of a linear coordinate transformation from resonator displacements to ellipsoidal deformations. This relationship is *not* general! In other arrangements of resonators, the equivalent resonator ellipsoids do not, in general, mimic the quadrupole ellipsoids, thus are not the same as mode channels. To produce mode channels for other arrangements, one would have to introduce the complicated frequency response described by Eq. (38).

VIII. A NEARLY TRUNCATED ICOSAHEDRAL ARRANGEMENT

We have seen how simple things become when the TI arrangement is used, but what happens if the system is not ideal? Using a numerical model, described below, we investigated the effects on the eigenfunctions due to perturbations of the system parameters. We found that small deviations of the various parameters (of the order 1%) from the ideal TI case did not significantly change the resonator ellipsoids. We therefore will discuss a situation where the tolerance on the parameters is relaxed to be of the order a few percent. In an actual experiment this is a rather poor level of precision; one expects to be able to do much better.

A. Normal mode coordinates

While all the signal information is contained in the resonator ellipsoids, it is useful to be able to transform the data to normal mode coordinates using Eq. (34) where the frequency response is simple. While not important for transforming between point radial coordinates to ellipsoidal coordinates, the symmetry breaking can be significant when transforming to normal mode coordinates.

To overcome this, we developed an *in situ* measurement technique [27] to determine the transformation matrix $\underline{\underline{V}}$. The transformation matrix can be measured by applying a continuous sinusoidal force anywhere on the sphere's surface at the frequency of one of the normal modes. (Note that this technique requires the normal modes to be *non-degenerate*, thus it is actually preferable to have a small amount of symmetry breaking.) The frequency response of the resonators will be simple because they are being driven at a single frequency. From Eq. (34) we see that the amplitude and phase of their response make up a single column of $\underline{\underline{V}}$. By exciting each normal mode in turn, the complete $\underline{\underline{V}}$ matrix can be measured. The only assumption made in calculating $\underline{\underline{V}}$ is that the resonators are "close" to the TI arrangement so that an ideal pattern matrix $\underline{\underline{B}}$ can be used and the quadrupole ellipsoids can be replaced by Eq. (46).

Once $\underline{\underline{V}}$ is measured the antenna can be operated to observe gravitational waves. The response of the resonators can be recorded and transformed to normal mode coordinates:

$$\underline{\eta} = \underline{\underline{V}}^{-1} \left[\begin{bmatrix} \underline{\underline{B}}\,\underline{q}_- \\ \underline{q}_- \end{bmatrix} + \begin{bmatrix} -\underline{\underline{B}}\,\underline{q}_+ \\ \underline{q}_+ \end{bmatrix} \right]. \tag{47}$$

Note that the resonator response must be bandpass filtered to separate the in-phase ($-$) and anti-phase ($+$) resonator ellipsoids. Since the frequency response of the normal modes is simple they can easily be fit for various parameters such as phase and amplitude. This information can then be transformed to mode channels using using Eq. (34). From the mode channels the direction and amplitude information of a possible gravitational wave event can be calculated as described above.

B. Numerical simulation of errors

1. Parameters

Now that we have written down the solutions to the equations of motion we can look at what are the parameters of the system and how uncertainties and deviations of them will affect a measurement. For the TIGA case we have the following parameters:

6	$\times$	k_j^r	resonator spring constants
5	$\times$	k_m^s	sphere mode spring constants
6	$\times$	ϕ_j	resonator positions
6	$\times$	θ_j	resonator positions
5	$\times$	β_m	sphere mode orientations
5	$\times$	γ_m	sphere mode orientations
6	$\times$	m_j^r	resonator masses
5	$\times$	m_m^s	quadrupole mode masses
6	$\times$	ϵ_j^r	resonator radial couplings
6	$\times$	ϵ_j^θ	resonator transverse couplings
6	$\times$	ϵ_j^φ	resonator transverse couplings

62 total parameters.

The angles β_m and γ_m describe the orientation of the quadrupole modes relative to a fixed lab frame, and will be discussed further below.

The parameters ϵ_j^r, ϵ_j^θ, and ϵ_j^φ are a measure of the coupling of the transducers to the radial and transverse motion of the sphere surface. In the above model we assumed $\epsilon_j^r = 1$ and $\epsilon_j^\theta = \epsilon_j^\varphi = 0$ because we felt their inclusion was unnecessary as transducers are currently available that do not strongly couple to transverse motion. However, it is useful to test this assumption and determine how strong a requirement should be set for the actual instrument. We include them here by replacing the pattern matrix defined by Eq. (18) with

$$B_{mj} \equiv \frac{1}{\alpha} \left(\epsilon_j^r \hat{\boldsymbol{r}} + \epsilon_j^\theta \hat{\boldsymbol{\theta}} + \epsilon_j^\varphi \hat{\boldsymbol{\varphi}} \right) \cdot \boldsymbol{\Psi}_m \left(\theta_j, \phi_j \right) \tag{48}$$

This should give a good approximation of the effects of transverse coupling, without the need of changing the model of the resonators from one dimensional harmonic oscillators. We considered these parameters as independent from each other. One might relate them with a parameter such as the angle between the transducer axis and the normal to the sphere surface, however we do not do this because for an actual resonant transducer there are several other mechanisms that can lead to transverse coupling, thus keeping these parameters independent seems reasonable.

Some of the above parameters can potentially be measured directly, such as the masses, however, we include them here for generality. In addition, the 5 quadrupole mode masses m_m^s would normally be set equal to each other and to the physical mass of the sphere, however, again for generality we kept it as a parameter. In the appendix we describe a procedure to measure most of these parameters, however the resonator ellipsoid method described above makes this unnecessary.

2. Simulation results

The transformation matrix $\underline{V}$ can be measured to very high accuracies, but our assumption that the resonator ellipsoids still mimic the sphere ellipsoids will have some error associated with it. This error will propagate through the analysis and into the results of a measurement. We, therefore, studied the effects of small perturbations to the above parameters on our ability to accurately determine the direction of an excitation.

We developed a Monte Carlo type simulation where we added a small random perturbation (uniform distribution) to the above parameters within a specified tolerance. We then simulated an excitation and calculated the direction using the resonator ellipsoid method. The direction calculation assumed the ideal case: it was not given knowledge of the true values of the parameters.

As shown in Fig. 3, the results of the numerical simulation indicate that a direction calculation becomes unreliable only after the tolerance of all the parameters exceeds about 3%. This is certainly an obtainable level of precision. Fig. 4 shows the solid angle estimation error $\Delta\Omega$ [28] for several tolerances. We also varied the location of the excitation, but found no significant difference in the results. Note that these are systematic errors due to the analyses technique, not random errors as the figures might imply.

To put these results into perspective, we compared these systematic errors to the random error due to a finite signal-to-noise ratio as calculated by Zhou and Michelson [12]. We find that one would need a signal-to-noise ratio of about 1000 in energy before our systematic errors become significant (choosing a tolerance of 2%). While one might hope to observe sources at this level, the most optimistic predictions lead to considerably smaller signal-to-noise ratios [29]. We, therefore, feel that the systematic errors are sufficiently low that there is no need to develop an alternative technique that requires precise knowledge of the parameters.

Looking at the individual contribution to the errors from each parameter we determined which were most dominant. We found that the most significant errors came from the resonator positions ϕ_j and θ_j. All the other parameters had associated errors at least one order of magnitude in $\Delta\Omega$ lower than those from the resonator positions for reasonable tolerance levels. This included the errors associated with the coupling parameters ϵ_j^r, ϵ_j^θ, and ϵ_j^φ, thus justifying our earlier decision to omit them from the model.

Perturbations to the sphere mode orientations β_m and γ_m did not lead to *any* errors! We expected that simple linear combination of the quadrupole modes do not lead to any error, however, what is surprising is that a direction calculation's ignorance of the true orientation in a non-degenerate system does not lead to any errors. This is important as it tells us that it is unnecessary to measure the mode orientation before equipping the sphere with resonant transducers (as was done on the prototype TIGA for other reasons discussed below). While these parameters may not completely describe the effects of deviations of the quadrupole modes from an ideal sphere, we found from measurements [22] that they are the dominant effect of symmetry breaking. The fact that they do not contribute *at all* to the errors on a measurement also frees us from putting strong constraints on the spherical mass. This allows us, for example, to put a hole through the center of the sphere for suspension purposes, or use a TI (or some other "spherical" shape) instead of a sphere.

IX. THE LSU PROTOTYPE TIGA

The above model outlines a clear algorithm for obtaining the gravitational amplitudes from a spherical antenna. However, like most models, we must evaluate its worth with an actual experiment. We therefore constructed a room temperature prototype TIGA. In the following sections we describe how the prototype was used to: first, verify that a TI has the same mode structure as a sphere; second, determine the effects of asymmetries on the sphere modes, such as a hole drilled through the center for suspension; third, verify the mode channel and ellipsoidal theories; and finally, verify the direction finding algorithms.

The prototype TI was machined from a bar of aluminum alloy 6063 that had previously been used as a cylindrical gravitational wave detector and was known to have good mechanical properties. Some key dimensions of the TI are shown in Fig. 5. The prototype had a center of mass suspension. A hole was bored along a diameter that started from the center of a hexagon face. The hole changed diameter just above the center of mass, and a thin titanium suspension rod, which widened to a cone at one end to mate with the hole's change in diameter, was inserted from the large diameter side.

The prototype was first suspended and tested without mechanical resonators attached. This testing gave many insights into the differences between an ideal sphere and a real one. The results of this testing was summarized elsewhere [22] but we include here some of the important results that are needed to describe the coupled system.

Once the uncoupled tests were completed, resonant transducers were attached, and the coupled system was studied. Preliminary results of these tests were also summarized elsewhere [27,30], but we report here the completed work in detail.

While we have attempted to report here as many of the important aspects of the experiment as possible, we have omitted many of the specifics of this particular apparatus; for those details we refer the reader to reference [21].

X. THE UNCOUPLED PROTOTYPE

A. Normal Mode Frequencies

The measured frequency spectrum of the uncoupled TI is shown in reference [22]. We were able to identify most of the predominant modes using solutions to the elastic equations of a sphere [31] and a finite element model of a TI [21]. We found the degeneracy of all multiplets to be lifted by a small amount: 1% or less in frequency. We were able to match the measured frequencies of most of the multiplets to the theory for a sphere to better than 1%.

The modes of most interest for gravitational wave detection are the 5 members of the lowest quadrupole mode multiplet near 3235 Hz. For a homogeneous isotropic sphere, those modes are exactly degenerate. We found that this quintuplet was split into two doublets and a singlet, spread over a range of 0.8% in frequency, as shown in Fig. 6. Additional data (not shown), confirmed that the two peaks labeled as doublets are each composed of two modes split by about 1 Hz.

Upon reflection, we realized that the suspension hole bored through the TI must be the primary cause for the splitting of the quintuplet. It breaks the spherical symmetry, but preserves cylindrical symmetry about the hole axis. The specific identification of the multiplets shown in Fig. 6 was surmised on physical grounds, and confirmed by measurements described below. We have not attempted to calculate the magnitude of the splitting caused by the hole, so we cannot make a comparison with the data, however, this effect has subsequently been confirmed by others [23].

B. Monopole Mode Calibration

This experiment dealt with high signal-to-noise ratios, and absolute energy calibration was unnecessary. However, it was important to know the relative sensitivity of the motion sensors and correct for any differences. The monopole, or breathing, mode of a sphere (which for this TI had a frequency near 6880 Hz) is a spherically symmetric radial expansion and contraction of the surface. The TI had no other modes close in frequency to the monopole mode. This made it ideal to measure the relative sensitivity of the motion sensors.

We excited vibrations of the TI with radial impulses from a hammer at various locations on the surface. Shown in Fig. 7, we found that the responses of the six motion sensors, at the monopole frequency, were identical in phase, and independent of the position of the impulse, but differed systematically in amplitude by up to 10%. These amplitude differences were due to the quality of the attachment of the motion sensors as well as gain differences in the electronics chain. These measured gain deviations were then used to correct the amplitudes in all the subsequent measurements.

This method proved to be very convenient as the motion sensors did not have to be removed or remounted, which was found to change their sensitivity.

C. Simple mode channels

We observed the quadrupole mode multiplet by sampling the motion of the TI at 6 discrete positions, using small, non-resonant, accelerometers waxed to the surface in the TI arrangement as shown in Fig. 1. According to the standard normal mode picture of vibrational mechanics, the free motion at these points, or any point on the surface, can be viewed as the combination, or superposition, of the response of the normal modes. Thus each motion sensor will record a different linear superposition of the responses of all the modes.

A hammer was used to impulsively excite vibrations of the sphere. Narrow-band filtering was used to isolate the quadrupole modes. The measured response of each motion sensor is shown in reference [22]. As expected, the non-degeneracy of the modes caused the individual sensor outputs to display the various modes beating against each other, making it difficult to make a *direct* estimate of the amplitude of each normal mode.

We showed above that the desired mode amplitudes could be separated out by combining the outputs of all the sensors in special linear combinations, whose coefficients were grouped together into the pattern matrix $\underline{B}$. We called these combinations "mode channels" to indicate they had a one-to-one correspondence with the quadrupole normal mode amplitudes of the sphere. For the case of the uncoupled prototype, we do not need to included the measurement of the matrix $\underline{V}$ to convert to normal modes, as the uncoupled sphere quadrupole modes *are* the normal modes, thus their frequency response is simple. In addition, for the case of *this prototype*, we could not use this procedure because several of the modes were nearly degenerate, thus exciting them individually with a simple sine-wave excitation was impossible.

To obtain nearly perfect mode channels, we rotated the spherical harmonics that determined the pattern matrix, until we found the best fit to a single frequency in each mode channel. We chose to use the y-convention for the Euler angles [32] to perform the rotations. The rotation α about the z-axis was not used because it had little effect on the fit. The β rotation about the new y-axis mixed mode 5 with the other 4 modes, while maintaining orthogonality. The γ rotation about the new z-axis mixed the new modes 1 with 2, and 3 with 4, but not 1 with 3 or 4, etc. Therefore, these rotation angles could be different for the two pairs and still maintain orthogonality. Mode 5 was unaffected by any γ rotation. The best fit values for the rotation angles from the lab coordinate system shown in Fig. 1 were $\gamma_{12} = -0.1$, $\gamma_{34} = -7.2$, and $\beta = 1.0$.

Each mode channel was well separated from the others and behaved as expected, an exponentially decaying sine wave. By examining the power spectrum, we determined that the residual amplitude of the "wrong" modes present in a channel was less than 2%. This small residual admixture may, or may not, be due to imprecise positioning of the accelerometers.

D. Simple impulse test

As a final test of the uncoupled system, we applied several radial impulses to the center of nine different faces of the TI, and then calculated the locations from the algorithm described above. The results of this comparison are shown in reference [22]. The locations calculated from the data were very consistent; with three hits at each location, the overall standard deviation from the mean was $\sim 0.4°$. The calculated locations were all within $\sim 3\%$ of the values expected from the measured geometric position of the impulse hammer. The deviation from the expected values is apparently a systematic error, perhaps from imprecise placement of the accelerometers or the impulse hammer. Below we describe the results of a similar test, but with the accelerometers replaced by resonant transducers.

E. Insights from the uncoupled prototype

Experiments on the uncoupled prototype showed that the departures from perfect spherical behavior and symmetry were not large. The quadrupole modes were no longer degenerate, but the source of their frequency splitting is understood. The eigenfunctions of the uncoupled TI were found to be unchanged in shape from those of a perfect sphere by an amount less than 2%; the main effect of the symmetry breaking was to fix them in a particular orientation. The simple impulse test confirmed the practicality of the direction finding technique. From these results, we conclude that a TI represents a good approximation for a sphere and is sufficient for use as an omnidirectional gravitational wave

antenna. Knowing these results, we were confident enough to instrument the prototype TI with resonant transducers to fully test the TIGA theory.

XI. THE PROTOTYPE WITH RESONANT TRANSDUCERS

A. Transducer design and attachment

Section IV lists the rudimentary requirements for a resonator, but practical considerations require a more extensive list. First, the "transducer mode" must be reasonably easy to tune to the quadrupole frequency. Second, the transducer mode must be purely radial, so that it couples strongly only to the radial motion of the quadrupole modes. Third, there should not be any other modes of the resonator nearby in frequency. Fourth, there must be a practical method of attachment with sufficient mechanical Q.

The design we adopted for the prototype, shown in Fig. 8, approximates a lumped mass and a spring. The lumped mass, or "head", is attached to a thin stem, or "neck." The neck is fixed to a base which is then attached to the surface of the prototype. These three parts were machined from a single piece of aluminum. The transducer mode is such that radial motion of the head compresses and extends the neck against the base. While the neck is relatively rigid in the radial direction, it is relatively flexible in the transverse directions, which decouples the transducer mode from transverse motions. While designing the resonator, the length and diameter of the neck can be adjusted to move the rocking and torsional modes of the resonator well below the transducer mode frequency.

A piezoelectric strain gauge was epoxied to the neck of each resonator. The strain induced in the crystal will be proportional to the change in length of the neck, thus providing an efficient way of observing the motion of the resonators. The output of the strain gauges were first demodulated to low frequency using 6 separate lock-in amplifiers, using the same reference, and then recorded on a high speed data acquisition system. The resonators and measurement system are described in detail in reference [21].

We used finite element analysis to fix the final parameters of the resonator. The final tuning of the resonators was done while attached to the TI. The equations of motion for this system are given in Sec. IV taking the number of resonators equal to one. We measured the coupled mode frequencies of the prototype and one resonator and compared them to the eigenvalue solution of Eq. (22) to determine the spring constant of the small resonator. We had two practical options for tuning the resonator: reduce the mass of the head, or lower the spring constant by reducing the diameter of the neck.

We attached the resonators to the prototype with epoxy. While this method may not lead to the best mechanical Q, we found it was sufficient. The coupled modes had a Q of about 10^3 in vacuum while the uncoupled sphere modes had a Q of about 10^4. We suspect this difference is due to the method of attachment. In air the coupled modes had a very poor Q, thus we felt it was necessary to perform all test of the coupled system under vacuum.

The resonators were attached to the prototype one at a time, and the frequencies of the coupled modes were measured after each change. The calculated and measured quadrupole mode frequencies were fairly consistent with each other. The non-degeneracy of the prototype's quadrupole modes did not introduce much deviation from a perfectly degenerate system. It was also found that neither the toroidal modes nor the monopole mode of the sphere were shifted by more than 1 Hz when the resonators were added. Fig. 9 shows the results of the frequency measurements of the coupled modes for each addition of a resonator. The results are compared with what is expected from the eigenvalue solution of Eq. (22) beginning with the measured uncoupled eigenfrequencies. The two sets are consistent within 0.2%. While we consider this very good agreement, Lobo and Serrano found slightly better agreement (possibly due to better numerical precision), with this data, by applying the equations of motion in an equivalent, but different form [11].

B. Transformation to normal modes

With the 6 resonators attached, we were ready to observe the sphere modes using the resonator ellipsoid technique. The first step was to measure the transfer function $\underline{V}$. We attached a simple non-resonant piezoelectric shaker to the surface of the prototype. The frequencies of the $1\overline{1}$ normal modes were accurately measured by driving the shaker with a single frequency sine-wave, adjusting the frequency until a maximum response of a single normal mode was observed. With this system in equilibrium, we recorded the response of the 6 resonators to the continuous wave excitation. The frequency of the excitation was then changed to measure the next normal mode frequency and the above steps repeated.

As shown in Fig. 10, the frequency response of the resonators was simple because we were driving at a single frequency. The amplitudes of their response made up a single column of $\underline{V}$. By exciting each normal mode in turn,

the complete transformation matrix was measured. We repeated this measurement for several different locations of the shaker, all of which gave consistent results.

Shown in Fig. 11 is the results of using the measured transformation matrix $\underline{V}$ to calculate the response of the normal modes to the normal mode excitation of Fig. 10. For this case the TI was driven with a continuous wave excitation at the frequency of the fifth normal mode. As shown in the figure, only the fifth normal mode was excited, as expected. Again, this experiment had high signal-to-noise ratios, thus the essentially flat lines of the non-excited modes actually represent a "leakage" level of about 5% in amplitude.

C. Impulse direction test

To combine the entire TIGA technique into a single test, we applied an impulse excitation to the surface of the prototype TIGA to determine if the location of the impulse can be measured from the response of the resonators. An impulsive force was applied to the surface of the TI by sending a short electrical pulse to a non-resonant piezoelectric shaker attached to the surface.

Shown in Fig. 12 is a typical response of the six transducers to an impulsive excitation. Following the technique described above, this data can be transformed to normal coordinates using the matrix $\underline{V}$. The results of this transformation to the data of Fig. 12 is shown in Fig. 13. As expected, the data separated into 11 channels, each containing a single frequency representing the response of a single normal mode. Since each channel contains only a single frequency, it is relatively easy to fit them for their phase and amplitude at the time of excitation. Once these quantities are found we can transform them to mode channels and compute the location of the impulse as described above.

The results of this analysis for the various impulse locations is shown in Fig. 14. The locations calculated from the data were very consistent; with several impulses at each location, the overall standard deviation from the mean was $0.1°$. On average, the calculated locations were all within $2.7°$ of the values expected from the geometrically measured position of the center of the shaker.

The deviation from the expected values can be accounted for by the accuracy of the excitation method. The shaker used to apply the impulsive force did not actually apply a "point" impulse, but rather one that was distributed over a ring about the circumference of the shaker. By systematically repositioning the shaker, we determined that the "true" location of the impulse was anywhere within $2.5°$ of the geometric center of the shaker. A more precise way of exciting the prototype would have been preferred, however, we found this method to be adequate to verify the principle of the technique.

XII. SUMMARY

Experiments on the prototype TIGA showed that the departures from ideal behavior were not large. In every case, ways could be found to handle the asymmetries without major difficulty, and to some extent they actually simplify the problem. A technique for determining the location of an external excitation, including that of a gravitational wave, from the motion sensor data was developed which, except for some bandpass filtering, is simply linear algebra. This makes its implementation simple in an automated data analysis system. The *in situ* measurement technique takes into account most deviations from perfect symmetry and the resulting transformation matrices enable the data to be transformed to a space where the frequency complications can be easily handled. The algorithm was tested on the prototype TIGA and was found to be consistent with the measured results within the accuracy of the experiment. Since all the techniques described can be applied *in situ*, they are directly applicable for use on a real spherical antenna searching for gravitational waves.

ACKNOWLEDGMENTS

APPENDIX: RESONATOR CHANNELS

To measure all the parameters of a spherical antenna *in situ* without introducing any new parameters we could do the following. Excite one of the resonators with an external force and measure the response of all the resonators. If we were to excite at some other location, this would introduce new unknown parameters such as the location of the excitor.

We assume that we have a high signal-to-noise ratio so that we can ignore any external forces acting directly on the sphere modes. We therefore can set the forces $\underline{F}^s = 0$. We now write Eqs. (36) and (37) as

$$\left(\underline{\underline{K}}^r - \omega^2 \underline{\underline{M}}^r\right) \underline{q}(\omega) - \alpha \omega^2 \underline{\underline{M}}^r \underline{\underline{B}}^T \underline{a}(\omega) = \underline{F}^r(\omega) \tag{A1}$$

$$\left(\underline{\underline{K}}^s - \omega^2 \underline{\underline{M}}^s\right) \underline{a}(\omega) - \alpha \underline{\underline{B}}\,\underline{\underline{K}}^r \underline{q}(\omega) = -\alpha \underline{\underline{B}}\,\underline{F}^r(\omega). \tag{A2}$$

Solving for $\underline{F}^r(\omega)$ in terms of the observable $\underline{q}(\omega)$ we find

$$\underline{F}^r(\omega) = \left[\underline{\underline{I}} - \alpha^2 \omega^2 \underline{\underline{M}}^r \underline{\underline{B}}^T \left(\underline{\underline{H}}^s(\omega)\right)^{-1} \underline{\underline{B}}\right]^{-1} \left[\underline{\underline{H}}^r(\omega) - \alpha^2 \omega^2 \underline{\underline{M}}^r \underline{\underline{B}}^T \left(\underline{\underline{H}}^s(\omega)\right)^{-1} \underline{\underline{B}}\,\underline{\underline{K}}^r\right] \underline{q}(\omega). \tag{A3}$$

For the case of an ideal TIGA Eq. (A3) can be further simplified:

$$\underline{F}^r(\omega) = \frac{\left(k_s - \omega^2 m_s\right)\left(k_r - \omega^2 m_r\right) - \frac{3}{2\pi}\alpha^2 \omega^2 m_r k_r}{\left(k_s - \omega^2 m_s\right) - \frac{3}{2\pi}\alpha^2 \omega^2 m_r} \underline{q}(\omega) \tag{A4}$$

One can imagine performing this experiment and then fitting the resulting data for the various parameters. However, during initial attempts to implement this technique we found the level of parameter fitting was complicated, even for advanced techniques such as simulated annealing, perhaps because global minimums did not exist. While it may be possible to accurately fit for these parameters, we preferred to avoid such a task by developing and implementing the method of resonator ellipsoids discussed above.

[1] K. S. Thorne, in *Three Hundred Years of Gravitation*, edited by S. W. Hawking and W. Israel (Cambridge University Press, Cambridge, 1987).
[2] A. Abramovici *et al.*, Science **256**, 325 (1992).
[3] E. Mauceli *et al.*, Physical Review D **54**, 1264 (1996).
[4] P. Astone *et al.*, Astroparticle Physics (In press).
[5] J. Weber, Physical Review **117**, 306 (1960).
[6] *Proceedings of the OMNI-1 workshop* (World Scientific Publishing Co. Pte. Ltd., Singapore, In press).
[7] R. V. Wagoner and H. J. Paik, in *Proceedings of International Symposium on Experimental Gravitation, Pavia* (Roma Accademia Nazionale dei Lincei, Roma, 1976), pp. 257–265.
[8] M. Bianchi *et al.*, Class. Quantum Grav. **13**, 2865 (1996).
[9] W. W. Johnson and S. M. Merkowitz, Physical Review Letters **70**, 2367 (1993).
[10] S. M. Merkowitz and W. W. Johnson, Physical Review D **51**, 2546 (1995).
[11] J. A. Lobo and M. A. Serrano, Europhysics Letters **35**, 253 (1996).
[12] C. Zhou and P. F. Michelson, Physical Review D **51**, 2517 (1995).
[13] T. R. Stevenson, in *First Edoardo Amaldi Conference on Gravitational Wave Experiments*, edited by E. Coccia, G. Pizzella, and F. Ronga (World Scientific Publishing Co., Singapore, 1995).
[14] T. R. Stevenson, in *Proceedings of the OMNI-1 workshop* [6].
[15] T. R. Stevenson, Physical Review D (In press).
[16] N. S. Magalhães, W. W. Johnson, C. Frajuca, and O. D. Aguiar, Monthly Notices of the Royal Astronomical Society **274**, 670 (1995).
[17] L. D. Landau and E. M. Lifshitz, *Theory of Elasticity*, 3rd ed. (Pergamon Press, New York, 1986).
[18] P. Jaerisch, J.f. Math. (Crelle) **Bd. 88**, (1880).
[19] H. Lamb, in *Proceedings of the London Mathematical Society* (1882), Vol. 13.
[20] N. Ashby and J. Dreitlein, Physical Review D **12**, 336 (1975).
[21] S. M. Merkowitz, Ph.D. thesis, Louisiana State University, 1995.

[22] S. M. Merkowitz and W. W. Johnson, Physical Review D **53**, 5377 (1996).

[23] E. Coccia *et al.*, Physics Letters A **219**, 263 (1996).

[24] D. M. Eardley *et al.*, Physical Review Letters **30**, 884 (1973).

[25] D. M. Eardley, D. L. Lee, and A. P. Lightman, Physical Review D **8**, 3308 (1973).

[26] C. W. Misner, K. S. Thorne, and J. Wheeler, *Gravitation* (W. H. Freeman & Co., San Francisco, 1973).

[27] S. M. Merkowitz and W. W. Johnson, in *Proceedings of the OMNI-1 workshop* [6].

[28] Y. Gürsel and M. Tinto, Physical Review D **40**, 3884 (1989).

[29] L. S. Finn, in *Proceedings of the OMNI-1 workshop* [6].

[30] S. M. Merkowitz and W. W. Johnson, submitted to Physics Letters A (unpublished).

[31] J. A. Lobo, Physical Review D **52**, 591 (1995).

[32] H. Goldstein, *Classical Mechanics*, 2nd ed. (Addison-Wesley Publishing Company, Reading, Massachusetts, 1980).

FIG. 1. The truncated icosahedral gravitational wave antenna (TIGA) with transducer locations indicated. The transducers lie at two polar angles, $\theta = 37.3773°$ and $79.1876°$. Their azimuthal angles are multiples of $60°$.

FIG. 2. The symmetry of a Truncated Icosahedron

FIG. 3. The results of a numerical simulation of the systematic error on a source direction measurement due to a finite tolerance on the system parameters. The simulated wave is linearly polarized with direction $\theta = 1$ rad, $\phi = 2$ rad. Each point represents a single direction measurement with the system parameters varied within the specified tolerance.

FIG. 4. The solid angle direction estimation error as a function of the tolerance on the system parameters. Each x represents the results of a 200 trial simulation for a single source direction with all the system parameters varied within the corresponding tolerance. Changing the source direction produced similar results.

FIG. 5. Schematic of the prototype Truncated Icosahedron.

FIG. 6. The fine structure of the power spectrum of an impulse excitation of the TI's first quadrupole mode multiplet. The five degenerate modes of an isotropic homogeneous sphere were split into two close doublets and a singlet. Each mode is identified with its corresponding spherical harmonic.

FIG. 7. The response of the six accelerometers to an impulse excitation of the monopole mode of the prototype TI. Since the coupling to this mode is the same for all the accelerometers, it can be used to adjust for any differences in gain between the accelerometers and their readout electronics.

FIG. 8. Schematic of the resonant transducer.

FIG. 9. Frequency measurements of the coupled modes for each addition of a resonator. The solid lines are the measured values and the dotted lines are the calculated. The lines that are double in height represent degenerate doublets.
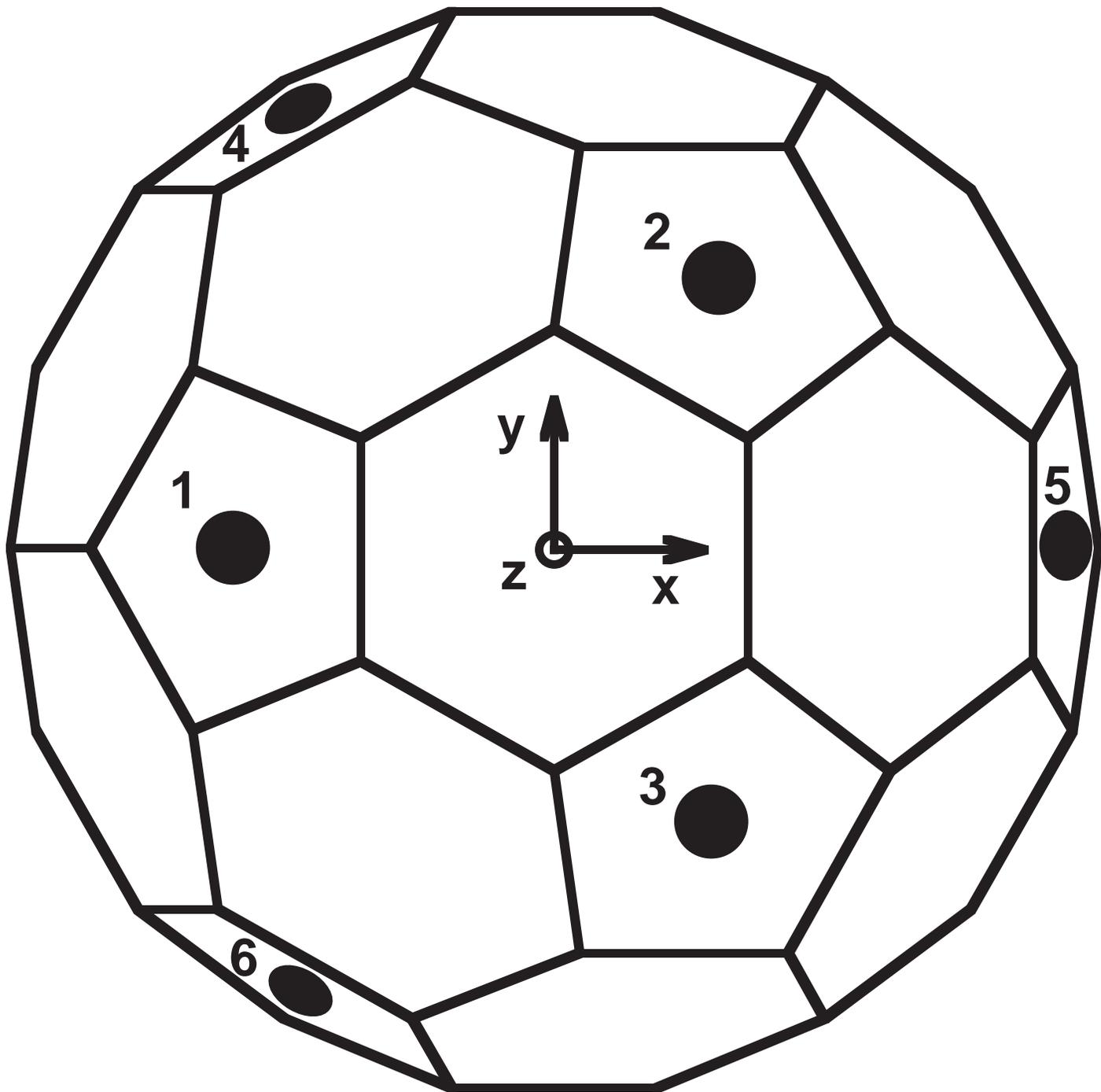
FIG. 10. A typical response of the six resonators to a continuous wave excitation applied to the surface of the prototype TI. The excitation for this case was at the frequency of the fifth normal mode. The outputs of the six resonant transducers was demodulated using 6 separate lock-in amplifiers using the same reference frequency at 3235 Hz (for clarity, only the in-phase is plotted).
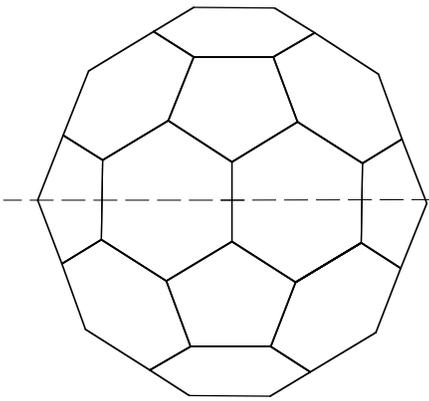
FIG. 11. The response of the 11 normal modes to a continuous wave excitation at the frequency of the fifth normal mode calculated from the data shown in Fig. 10. As expected, only the fifth normal mode shows a large response.

FIG. 12. A typical response of the six resonant transducers to an impulsive excitation applied to the surface of the prototype TI at time $t = 0$. The outputs of the six resonant transducers was demodulated using 6 separate lock-in amplifiers using the same reference frequency at 3235 Hz (for clarity, only the in-phase is plotted). The irregular response indicates that several normal modes contribute to the motion.
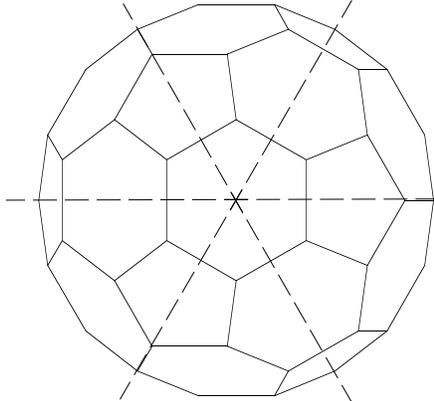
FIG. 13. The response of the 11 normal modes to an impulse excitation applied to the surface of the prototype TI at time $t = 0$, calculated by a linear combination of the data shown in Fig. 12. The regular response indicates that each channel corresponds to a single normal mode.

FIG. 14. Location of several impulses applied to the prototype TIGA. The x's mark the locations calculated from the motion sensor data, and the nearby o's mark the location of the center of the shaker measured geometrically.

2-fold   3-fold   5-fold

Top View

6.75"

Cross Section

138.18°

142.61°

1"

1.5"

30.65"

Front View

2.09"

3/4"

1/2"

Piezoelectric strain gauge

Base epoxied to TI

Top View

Ø2.36

Ø 3/8"